Real-time Blind Deblurring Based on Lightweight Deep-Wiener-Network

1st Runjia Li
Department of Engineering
University of Oxford
runjia.li@st-hughs.ox.ac.uk

2nd Yang Yu
Kuang Yaming Honors School
Nanjing University
191840314@smail.nju.edu.cn

3rd Charlie Haywood
Interlake High School
s-haywoodc@bsd405.org

***Abstract*—In this paper, we address the problem of blind deblurring with high efficiency. We propose a set of lightweight deep-wiener-network to finish the task with real-time speed. The Network contains a deep neural network for estimating parameters of wiener networks and a wiener network for deblurring. Experimental evaluations show that our approaches have an edge on State of the Art in terms of inference times and numbers of parameters. Two of our models can reach a speed of 100 images per second, which is qualified for real-time deblurring. Further research may focus on some real-world applications of deblurring with our models.**

***Index Terms*—Blind Deblurring, Wiener Filter, Deep Learning**

I. Introduction

Image deblurring has long been a popular area of computer vision, which aims at recovering the sharp version of blurred images. Several reasons may lead to blurring, such as the motion of the camera and out-of-focus, which can be represented as a blur kernel in the math form.

Different methods are applied for this task. The non-artificial intelligence methods mainly focus on finding an inverse function or filter to restore a sharp image from the original one. Multiple algorithms have been developed to address the problem, such as Lucy-Richardson [1] [2] and Wiener deconvolution [3] for non-blind deblurring, and maximum likelihood restoration [4] and deconvolution [5] for blind deblurring. Due to complicated blurring kernels from combined types of reasons, traditional methods often have difficulty dealing with real-world problems.

With the development of artificial intelligence, deep learning-based methods gain popularity in deblurring tasks with incomparable accuracy. Network architectures such as CNN [6], UNet [7], and GAN [8] have been widely used in this field. While they achieve high-quality restoration, the drawback of inference time and the number of parameters prevent these models from being applied to real-world situations.

In this study, we propose a set of lightweight deep-wiener-network to finish the task with real-time speed, which fills the gap of the artificial intelligence-based method for efficient deblurring tasks to the best of our knowledge. Our contributions here are: (a) we discuss the possibility of applying the wiener filter in blind deblurring combined with the deep neural network. (b) we compare the PSNR, inference time, and parameters among our models and some State of the Art. According to the experiments, our networks can reach the restoration performance nearly as well as some State of the Art, while also having a much shorter inference time of almost 0.01 seconds per image.

II. Related Works

A. Blind and Non-blind deblurring

Processes for image deblurring are separated into two categories: blind and non-blind deblurring. The former, blind motion deblurring, is responsible for estimating the blur kernel in an image, whereas the latter, non-blind deblurring, is meant to restore an image to its original quality using a provided blur kernel [9]. In current blind deblurring methods, algorithms will attempt to recover parameters of the kernel as it is significantly smaller in size compared to the image itself [10]. Blind deblurring as a technique is notably useful as it can be applied to scenarios in which the blur kernel's exact formula is unknown in advance. The applications of blind deblurring range from motion deblurring to clarify images of faces for biometrical analysis [11], Magnetic Resonance Image (MRI) deblurring caused by gaussian blur, out-of-focus imaging tools, motion blur, and more [12], as well as simple motion blur caused by the unsteady hand of a photographer.

B. Methods for Blind Image Deblurring

Given the assumption that the blur kernel is in a simpler parametric form such as a Gaussian form or low-frequency Fourier components, the task of deblurring can be easily approached. However, in real-world applications, blur kernels are far more complex due to the factors that can affect the blurring of an image. Thus, various alternate algorithms have implemented deep learning to capture the complexity of the deblur kernel, counteracting the blurring from equipment error.

One of such methods utilizes the maximum a-posteriori (MAP) solution to infer the parameters of the kernel and latent image gradients, which are then used in conjunction with the Richardson-Lucy algorithm to reconstruct the image. This method for reconstruction iteratively maximizes the likelihood function of a Poisson statistics image noise model, as well as only outputs the non-negative values [13]. Another existing method is ForWaRD, standing for Fourier-wavelet regularized deconvolution, which performs a scalar shrinking in both the fourier and wavelet domains, optimizing the mean squared

error (MSE) through the shrinkage of domains to result in more economical wavelet representations that require less Fourier shrinkage [14].

Jump Regression Analysis (JRA) is a multi-step deblurring model used to perform blind image deblurring that takes into account that the effects of blurring are influenced by location. To address this, a defined jump regression surface with various edges corresponding with the surface and its higher order derivatives' "jumps" is implemented through JRA. This method is successful in addressing the hierarchical nature of image deblurring, where JRA enables the ability for elements of the regression surface to be unrestricted based on predetermined assumptions [15].

Most recently, a method by the name of maximum entropy on the mean (MEM) has been developed based on the principle of maximum entropy (ME) developed in 1957, which is a method for estimating the optimal probability distribution [16]. The ME method can be used in deblurring, where each pixel's gray level is interpreted as a probability, and the image will be normalized, setting the values to sum to one, which can be followed by the application of the principle of maximum entropy under available constraints [17]. However, the MEM method starts with the utilization of vectors instead of a probability, where the pixelated image is considered as a random vector, where the principle of the ME is applied to the probability distribution of said vector. Available constraints are then imposed on the unknown probability distribution, becoming the constraints on the probability of the image. The MEM approach has an advantage over the traditional ME method in the avenue of flexibility, where the potential for implementation of nonlinear constraints.

Other existing reports make use of hyper-laplacian priors, modeled by a hyper-laplacian $p(x) \propto e - k|x|$ which was able to deconvolute a 1 megapixel image in less than 3 seconds using a lookup table, as compared to the iteratively reweighted least squares (IRLS) that takes 20 minutes for an image of comparable size [18]. The IRLS algorithm is used for calculating quantities of statistical interest using weighted least squares calculations iteratively [19] and can be applied to approach the task of blind deblurring. The IRLS algorithm has also been accelerated by a preconditioned conjugate gradient method, which is an effective method for solving a system of linear equations under the conditions that the coefficient matrix is symmetric and positive definite [20]. As a result, this was able to match the traditional IRLS model's time, and improve upon its computational cost efficiency for each iteration [21].

C. Blind deblurring with Deep Learning

Deep learning-based models like CNN (convolutional neural network) and DAE (deep auto-encoder)have developed fast in recent years and become efficient in image deblurring, denoising, and super-resolution.

Specifically for image deblurring, an early model MRFCNN [23] utilized a CNN-based structure to predict a multi-regional blur kernel for an image and deconvolute each region. MT-RNN [31] proposes incremental temporal training with constructed multi-temporal level dataset to replace multi-scale approaches.

DeepDeblur [25] uses a more straightforward approach with an end-to-end DAE (deep auto-encoder) structure, predicting the clear image directly from an input of blurred image in the spatial domain. The authors of DeepDeblur [25] innovate a residual block specifically for image deblurring. BIDN [26] also uses a DAE structure to obtain a blur invariant representation with regression over encoder-features, which is fed into a decoder to generate the clear image. Another DAE structure model MIMO-UNet [29] introduces a coarse-to-fine strategy and asymmetric feature fusion, which mimics multi-cascaded U-nets.

MPRNet [28] utilizes channel attention blocks and a multi-stage architecture, that progressively learns restoration functions for the degraded inputs, which enables the MPRNet to achieve the highest PSNR (peak signal-to-noise ratio) on GoPro dataset without further information from the frequency domain. NDeblur [24] trains a network to predict region-specific deconvolution filter in the frequency domain directly from the spatial domain without regularization on the filter. DeepRFT [33] introduces a residual fast Fourier Transform with convolution block to capture both high and low frequency information.

Various effective GAN(generative adversarial network)-based deblurring methods are also proposed to solve image deblurring problems. DeblurGAN [27] introduces a generative model to predict clear image based on conditional GAN and content loss. DBGAN [32] learns to blur and deblur images with GAN at the same time to address the problem that synthetic blurred and clear image pairs do not represent the blurring process faithfully in real world.

III. Theoretical Basement

A. 2D Fourier Transform

Fourier Transform as described in equation (1) converts geometrical information $f(x, y)$, where x, y denotes the pixel position, in the spatial domain (intensity value on different pixels of an image) into the frequency domain $F(u, v)$, where u, v denotes the spatial frequency. The process is based on the orthogonality of different spatial frequencies so that we can extract the magnitude distribution of the frequency domain with equation (1).

Equation (2) describes how the spatial information can be restored from different frequency components u and v. In other words, the spatial representations $f(x, y)$ and $F(u, v)$ are equivalent and contain the same information but in different forms.

$$F(u,v) = \int_{-\infty}^{\infty}\int_{-\infty}^{\infty} f(x,y) \cdot e^{-j2\pi\cdot(ux+vy)} dxdy \quad (1)$$

$$f(x,y) = \int_{-\infty}^{\infty}\int_{-\infty}^{\infty} F(u,v) \cdot e^{j2\pi\cdot(ux+vy)} dudv \quad (2)$$

One desired property of the Fourier Transform is that convolution (denoted as $*$ in this paper) in the spatial domain is equivalent to multiplication in the frequency domain as described by equation (3)

$$f_1(x,y) * f_2(x,y) = F_1(u,v) \cdot F_2(u,v) \tag{3}$$

B. Wiener Filter

A blurred image $b(x,y)$ is mathematically modelled to be a clear image $c(x,y)$ convoluted with a blur kernel $h(x,y)$ plus a noise $n(x,y)$ as described by equation (4). In reality, the noise could be from the environment when capturing the image or from the sensor of the camera. The noise tends to be spread out a wide range of frequencies but tend to be minor without manipulation.

And in frequency domain, the convolution becomes multiplication as described by equation (5).

$$b(x,y) = c(x,y) * h(x,y) + n(x,y) \tag{4}$$

$$B(u,v) = C(u,v) \cdot H(u,v) + N(u,v) \tag{5}$$

The multiplication-convolution duality enables image deblurring to be more efficient because calculating multiplication and division is much easier and faster for both human beings and computer than convolution and deconvolution.

In the frequency domain, if the noise term is neglected, it can be easily inferred that the restored clear image could be obtained by $C^{'}(u,v) = \frac{B(u,v)}{H(u,v)}$, which is called an Inverse Filter. However, the blur kernel $H(u,v)$ tends to be a low-pass filter in most cases and the inverse of a low-pass filter $\frac{1}{H(u,v)}$will be a high pass filter, which amplifies high frequency components. If we take the noise term into account, the restored image becomes $C^{'}(u,v) = \frac{C(u,v)\cdot H(u,v)+N(u,v)}{H(u,v)} = C(u,v)+\frac{N(u,v)}{H(u,v)}$. Thus, the high-frequency noise will be significantly amplified and the clear image cannot be restored if we directly apply the Inverse Filter.

Therefore, Wiener Filter $W(u,v)$ (equation (6)) is introduced to restore the original image as $C(u,v) = W(u,v) \cdot B(u,v)$, where $K(u,v)$ is theoretically the noise-to-signal-power ratio of the blurred image but in reality estimated by engineers.

$$W(u,v) = \frac{H^*(u,v)}{|H(u,v)|^2 + K(u,v)} \tag{6}$$

The intuition behind the Wiener Filter is that when $H(u,v) >> K(u,v)$ at low frequency since $H(u,v)$ is a low-pass filter, the Wiener Filter simply becomes an Inverse Filter and restore signals at low frequency faithfully. When $H(u,v) << K(u,v)$ at high frequency, $W(u,v) \to \frac{H^*(u,v)}{K(u,v)}$, which keeps decreasing as $H(u,v)$ decreases. Thus, Wiener Filter restores the image faithfully while prevents high-frequency noise corrupting the restoration process.

Wiener Filter is widely used and proved to be one of the most efficient method in traditional robotics odometry and SLAM.

C. Convolutional Neural Networks

Convolutinal Neural Networks (CNN) are generally made up of stacks of convolution layer, pooling layer, and fully-connected layer.

The convolution layer seems similar to traditional filtering but with a learnable kernel to convolute the input feature map and output the further extracted and abstracted features. Intuitively speaking, the deeper the layers the more abstracted features are represented in the intermediate feature maps (hidden image between layers) [34].

The pooling layer is fundamentally a down-sampling process involving various pooling techniques including max pooling, average pooling, and global pooling. The pooling layer reduces the resolution or channel of the processed intermediate feature map. For example, an $n \times n$ max pooling layer divides the intermediate feature map into several $n \times n$ patches and only passes the maximum value in one patch to represent the whole patch in the hidden output (next intermediate feature map). Thus, the feature map resolution will decrease by n^2 after the max pooling layer. The same logistics apply to average pooling and global pooling. Pooling layer reduces the intermediate feature map memory and therefore enables the CNN to be trained on limited computational resources. Besides, pooling gives the CNN model shift invariance and robustness to a certain degree [34].

The fully-connected layer usually appears in the last few layers of CNN classifiers, which consists of neuron units disposed of in interconnected multilayers like Multiple Layer Perceptron. The input of the fully-connected layer consists of all flatten feature maps from the last convolution layer and the output could be a feature vector or classification scores after SoftMax [34].

In summary, the CNN model extracts representative features from the input image for various tasks like classification, detection, and segmentation.

D. U-Net

U-Net adopts full convolution neural network After the image is input into U-net, it is down-sampled through convolution and pooling layers. After down sampling to a certain extent, the low-dimensional features will be up-sampled with up-convolution later to obtain higher resolution feature maps. During up-sampling feature maps with various resolutions during down-sampling are concatenated to the feature map during up-sampling before the next up-convolution layer. Finally, the feature maps are up-sampled and reconstructed to the original input resolution with a number of features extracted at various scales during down-sampling and up-sampling [35]. U-Net performs well on medical segmentation tasks and is now generalized to other computer vision tasks such as deblurring and diffusion model.

IV. Proposed Method

In the case of blind deblurring, the parameters $H(u,v)$ and $K(u,v)$ are traditionally hand-designed by engineers based on their prior knowledge when looking at the blurred image.

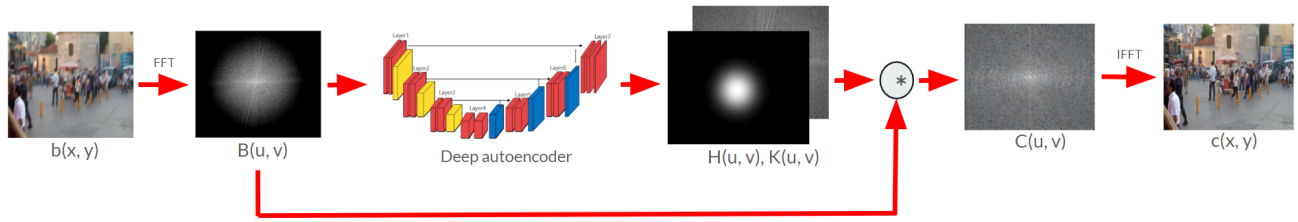

Fig. 1: DAE-based Wiener Filter

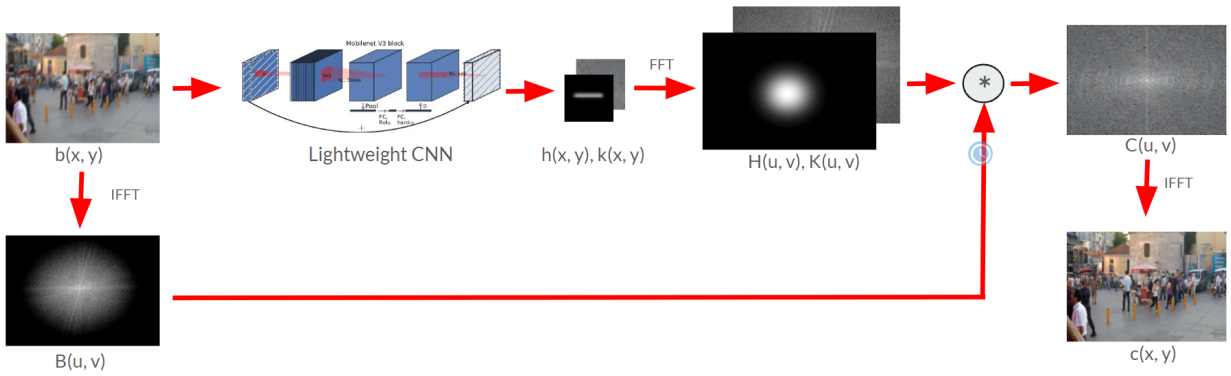

Fig. 2: Lightweight-CNN-based Wiener Filter

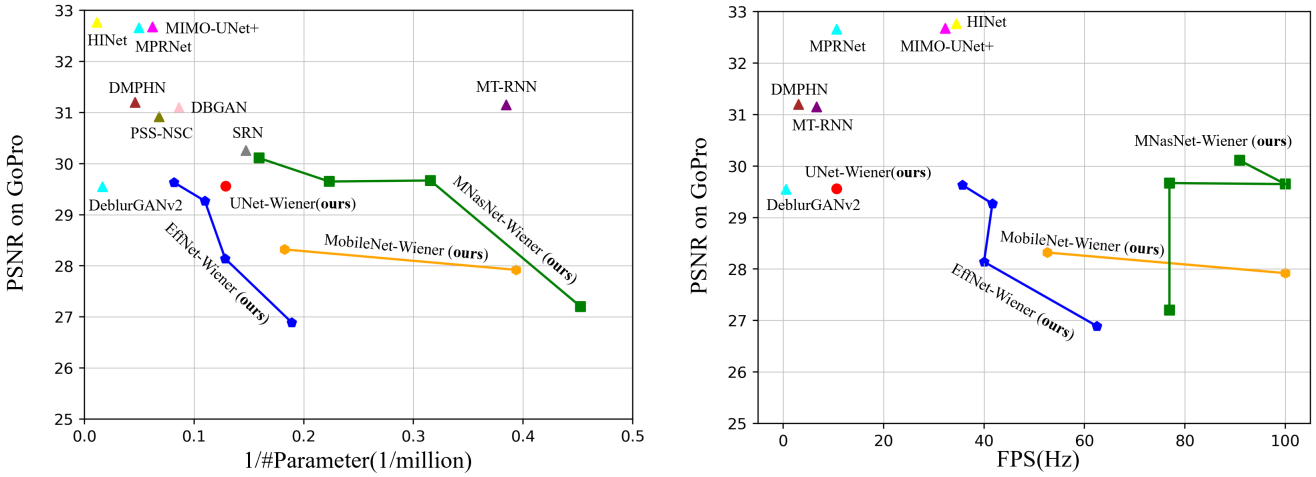

Fig. 3: PSNR vs. number of parameters (left) and FPS (right)

However, noise tends to be complicated and sometimes non-intuitive to correspond to a blur kernel. Therefore, we propose the deep-learning-based Wiener Network to learn to map from a blurred image to its most fitted Wiener Filter.

Our model aims to achieve better $\frac{PSNR}{Time}$ and $\frac{PSNR}{\#Parameter}$ than other state-of-the-art deblurring models so that real-time deblurring could be deployed on machines with limited computational resources such as embedded computer on UAVs or automobiles. Therefore we choose to use lightweight backbone models such as U-Net [35], MobileNetV3 [36], EfficientNet [37], and MNasNet [38].

A. *Deep Auto-encoder Wiener Filter*

As visualized in Fig. 1, The deep auto-encoder Wiener Filter first converts the input blurred image into the frequency domain by fast Fourier transform because the Wiener Filter parameters $H(u, v)$ and $K(u, v)$ are more directly related to the blurred image with frequency representation $B(u, v)$. Then the deep auto-encoder outputs the predicted Wiener Filter to deblur our input image in the frequency domain. Finally, inverse fast Fourier Transform is applied to the deblurred image with frequency representation and generate the actual

Model	PSNR	#Parameter	Time	$\frac{PSNR}{\#Parameter}$	$\frac{PSNR}{Time}$
MPRNet	32.66	20.1	0.094	1.625	349.08
MIMO-UNet+	32.68	16.1	0.031	2.030	1040.20
HINNet	**32.77**	88.7	0.029	0.369	1132.34
MT-RNN	31.15	2.6	0.151	11.981	206.31
DeblurGAN	29.55	60.9	1.826	0.485	16.18
DBGAN	31.10	11.6	0.297	2.681	104.71
DeepRFT	32.82	9.6	0.711	3.419	46.16
UNet-Wiener	29.56	7.8	0.094	3.809	314.47
MobileNetV3Small-Wiener	27.92	2.5	**0.010**	10.992	2820.20
MobileNetV3-Wiener	28.32	5.5	0.019	5.168	1490.52
MNasNet0-5-Wiener	27.20	**2.2**	0.013	**12.308**	2092.38
MNasNet0-75-Wiener	29.67	3.2	0.013	9.360	2282.31
MNasNet1-0-Wiener	29.65	4.4	**0.010**	6.769	**2906.86**
MNasNet1-3-Wiener	30.11	6.3	0.011	4.795	2737.27
EfficientNetB0-Wiener	26.89	5.3	0.016	5.083	1680.63
EfficientNetB1-Wiener	28.14	7.8	0.025	3.612	1125.60
EfficientNetB2-Wiener	29.27	9.1	0.024	3.213	1219.58
EfficientNetB3-Wiener	29.63	12.2	0.028	2.423	1058.21

TABLE I: Experiment result. We compared our deep learning-based wiener filters with some SOTA on different metrics. The names of our models are explained in the EXPERIMENT section.

deblurred image

We use U-Net as the deep auto-encoder in the pipeline and the model learned to minimize the mean squared error between the deblurred image by the predicted Wiener Filter and the clear image label.

B. CNN Wiener Filter

As visualized in Fig. 2, the lightweight CNN based Wiener Filter learns to predict the parameters in the Wiener Filter in similar way as the deep auto-encoder Wiener Filter but in the spatial domain first and converts the predicted Wiener Filter into the frequency domain to conduct the deblurring process.

The lightweight CNN Wiener Filter design proves to be more efficient than the deep auto-encoder potentially because the deep-learning models are more suitable at dealing with real number data in the spatial domain than complex number daya in the frequency domain. Besides, from the experiment section below, the CNN Wiener Filter is proven to be more efficient than most of the state-of-the-art models

V. Experiment

A. Dataset

In this experiment, we use a dataset called GoPro [39] to evaluate the performance of deblurring (PSNR) and computational efficiency (FPS) of different deep neural networks. It contains 2103 samples of blurry images and 1111 samples for testing. Considering the limited computational resource, we conduct experiments on 16 image pairs on each model three times and calculate their mean PSNR and FPS as the final results.

B. Implementation Details

Generally, We apply several different versions of U-Net, MobileNetV3, EfficientNet, and MNasNet in our experiments. We use PyTorch for the implementation of these models.

1) **U-Net** The U-Net contains a traditional structure of 12 down-sample layers and 12 up-sample layers. All of them have a kernel size of 3 with stride 1.
2) **MobileNetV3** In this experiment, we use both small and large versions of MobileNetV3 provided by the authors. They have the same network structure with some differences in the numbers of bneck. They are named as *MobileNetV3* and *MobileNetV3Small* mentioned in Table I.
3) **EfficientNet** We apply four EfficientNets for the backbone, which differ in their depth, width, and resolution. *EfficientNetB0*, *EfficientNetB1*, *EfficientNetB2*, and *EfficientNetB3* in Table I indicate different versions of EfficientNet.
4) **MNasNet** We also apply four MNasNet for the backbone. They have some differences in their depth.*MNasNet0-5*, *MNasNet0-75*, *MNasNet1-0*, and *MNasNet1-3* in Table I refer to different depth multipliers for MNasNet.

All experiments are conducted on Colab, with an input size of 1280×720, on an NVIDIA K80 GPU.

C. Result

We show the result of our deep neural network-based wiener filter in Table I. We compared several metrics mentioned above with some State of the Art. Overall, our models perform favorably compared with other methods in terms of efficiency with a relatively small amount of loss in accuracy.

Especially, for inference time, both *MobileNetV3Small-Wiener* and *MNasNet1-0-Wiener* reach the fastest processing speed of 0.01s per image, which is far more efficient compared with SOTA. The speed of almost 100 fps enables our model to achieve real-time deblurring for sophisticated real-world tasks.

In addition, we also compare the $\frac{PSNR}{\#Parameter}$ and $\frac{PSNR}{Time}$ among these models, which evaluates both their efficiency and accuracy. For the former one, *MNasNet0-5-Wiener* achieves

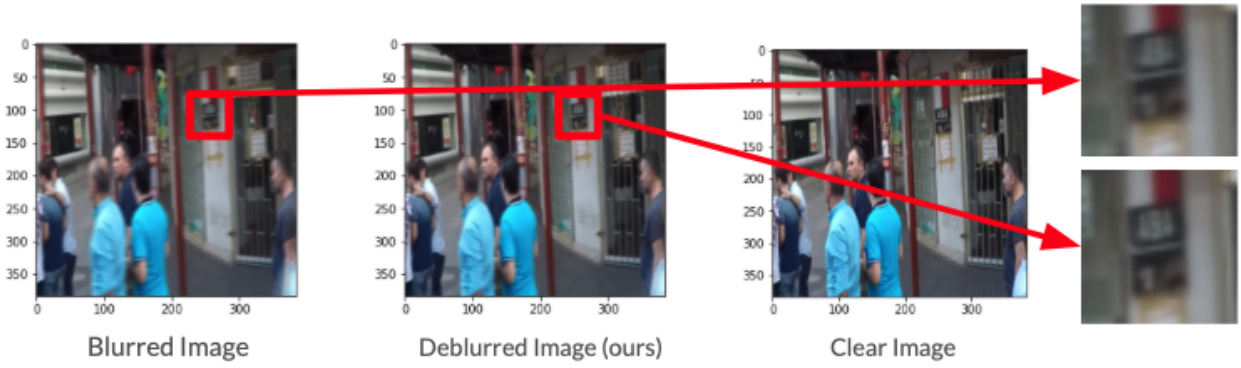

Fig. 4: Deblurred Image Demonstration from GoPro Dataset

the highest value of nearly 12.31. The performance reflects the model's advantage of easy deployment to hardware devices. For the latter one, *MNasNet1-0-Wiener* reaches the highest value of 29.07. As a result, the model is able to perform nearly as well as state of the art, while having an edge on them in efficiency. Generally, our models obtain considerable improvement over some SOTA. The result is illustrated more vividly in Fig. 3.

VI. Conclusion

In this paper, we discuss the effects of using deep learning-based wiener filter in image deblurring task. We use four different types of neural network as backbone, and design a pipeline for deep auto-encoder wiener filter. According to our experiments, we achieve an improvement of inference time and efficient compared with SOTA. It proves that our model will be useful for application in this field.

References

[1] L. B. Lucy. "An iterative technique for the rectification of observed distributions." The Astronom. Journal, 79:745, 1974.

[2] W. Richardson. "Bayesian-based iterative method of image restoration." J. Opt. Soc. America, 62(1):55–59, 1972.

[3] N. Wiener and C. Mathematician, "Extrapolation, interpolation, and smoothing of stationary time series: with engineering applications", vol. 21, 113 vols. MIT press Cambridge, MA, 1949.

[4] Y. Vardi and D. Lee, "From Image Deblurring to Optimal Investments: Maximum Likelihood Solutions for Positive Linear Inverse Problems," Journal of the Royal Statistical Society: Series B (Methodological), vol. 55, no. 3, pp. 569–598, 1993, doi: 10.1111/j.2517-6161.1993.tb01925.x.

[5] C. Byrne, "Iterative algorithms for deblurring and deconvolution with constraints," Inverse Problems, vol. 14, no. 6, p. 1455, Dec. 1998, doi: 10.1088/0266-5611/14/6/006.

[6] C. J. Schuler, M. Hirsch, S. Harmeling, and B. Schölkopf, "Learning to Deblur." arXiv, Jun. 28, 2014. Accessed: Nov. 27, 2022. [Online]. Available: http://arxiv.org/abs/1406.7444

[7] D. Ren, K. Zhang, Q. Wang, Q. Hu, and W. Zuo, "Neural Blind Deconvolution Using Deep Priors," in 2020 IEEE/CVF Conference on Computer Vision and Pattern Recognition (CVPR), Seattle, WA, USA, Jun. 2020, pp. 3338–3347. doi: 10.1109/CVPR42600.2020.00340.

[8] O. Kupyn, V. Budzan, M. Mykhailych, D. Mishkin, and J. Matas, "DeblurGAN: Blind Motion Deblurring Using Conditional Adversarial Networks," in 2018 IEEE/CVF Conference on Computer Vision and Pattern Recognition, Salt Lake City, UT, Jun. 2018, pp. 8183–8192. doi: 10.1109/CVPR.2018.00854.

[9] S. Vasu, V. R. Maligireddy and A. N. Rajagopalan, "Non-blind Deblurring: Handling Kernel Uncertainty with CNNs," 2018 IEEE/CVF Conference on Computer Vision and Pattern Recognition, 2018, pp. 3272-3281, doi: 10.1109/CVPR.2018.00345.

[10] A. Levin, Y. Weiss, F. Durand and W. T. Freeman, "Understanding and evaluating blind deconvolution algorithms," 2009 IEEE Conference on Computer Vision and Pattern Recognition, 2009, pp. 1964-1971, doi: 10.1109/CVPR.2009.5206815.

[11] F. Alaoui, A. Ghlaifan, D. Vamara, and N. Abdelkarim. Ap-plication of Blind Deblurring Algorithm for Face Biometric.International Journal of Computer Applications, 105:0975 –8887, 11 2014

[12] S. Agarwal, O. P. Singh, and D. Nagaria, "Deblurring of MRI image using blind and non-blind deconvolution methods," Biomedical and Pharmacology Journal, vol. 10, no. 3, pp. 1409–1413, 2017.

[13] R. Fergus, B. Singh, A. Hertzmann, S. T. Roweis, and W. T. Freeman, "Removing Camera Shake from a Single Photograph," p. 8.

[14] R. Neelamani, Hyeokho Choi and R. Baraniuk, "ForWaRD: Fourier-wavelet regularized deconvolution for ill-conditioned systems," in IEEE Transactions on Signal Processing, vol. 52, no. 2, pp. 418-433, Feb. 2004, doi: 10.1109/TSP.2003.821103.

[15] P. Qiu and Y. Kang, "Blind Image Deblurring Using Jump Regression Analysis," Statistica Sinica, vol. 25, no. 3, pp. 879–899, 2015.

[16] E. T. Jaynes, "Information Theory and Statistical Mechanics," Phys. Rev., vol. 106, no. 4, pp. 620–630, May 1957, doi: 10.1103/PhysRev.106.620.

[17] G. Rioux, R. Choksi, T. Hoheisel, P. Marechal, and C. Scarvelis, "The Maximum Entropy on the Mean Method for Image Deblurring," Inverse Problems, Oct. 2020, doi: 10.1088/1361-6420/abc32e.

[18] D. Krishnan and R. Fergus, "Fast Image Deconvolution using Hyper-Laplacian Priors," in Advances in Neural Information Processing Systems, 2009, vol. 22. Accessed: Nov. 26, 2022.

[19] M. Jorgensen, "Iteratively Reweighted Least Squares," in Encyclopedia of Environmetrics, John Wiley & Sons, Ltd, 2006. doi: 10.1002/9780470057339.vai022.

[20] S. C. Eisenstat, "Efficient Implementation of a Class of Preconditioned Conjugate Gradient Methods," SIAM J. Sci. and Stat. Comput., vol. 2, no. 1, pp. 1–4, Mar. 1981, doi: 10.1137/0902001.

[21] C. Chen, J. Huang, L. He, and H. Li, "Fast Iteratively Reweighted Least Squares Algorithms for Analysis-Based Sparsity Reconstruction." arXiv, Apr. 28, 2015.

[22] H. Miao, W. Zhang and J. Bai, "Aggregated Dilated Convolutions for Efficient Motion Deblurring," 2018 IEEE International Conference on Multimedia and Expo (ICME), 2018, pp. 1-6, doi: 10.1109/ICME.2018.8486567.

[23] J. Sun, W. Cao, Z. Xu, and J. Ponce, "Learning a Convolutional Neural Network for Non-uniform Motion Blur Removal." arXiv, Apr. 12, 2015.
[24] A. Chakrabarti, "A Neural Approach to Blind Motion Deblurring." arXiv, Aug. 01, 2016.
[25] S. Nah, T. H. Kim, and K. M. Lee, "Deep Multi-scale Convolutional Neural Network for Dynamic Scene Deblurring," in 2017 IEEE Conference on Computer Vision and Pattern Recognition (CVPR), Honolulu, HI, Jul. 2017, pp. 257–265. doi: 10.1109/CVPR.2017.35.
[26] T. M. Nimisha, A. K. Singh, and A. N. Rajagopalan, "Blur-Invariant Deep Learning for Blind-Deblurring," in 2017 IEEE International Conference on Computer Vision (ICCV), Venice, Oct. 2017, pp. 4762–4770. doi: 10.1109/ICCV.2017.509.
[27] O. Kupyn, V. Budzan, M. Mykhailych, D. Mishkin, and J. Matas, "DeblurGAN: Blind Motion Deblurring Using Conditional Adversarial Networks." arXiv, Apr. 03, 2018.
[28] S. W. Zamir et al., "Multi-Stage Progressive Image Restoration," in 2021 IEEE/CVF Conference on Computer Vision and Pattern Recognition (CVPR), Nashville, TN, USA, Jun. 2021, pp. 14816–14826. doi: 10.1109/CVPR46437.2021.01458.
[29] S.-J. Cho, S.-W. Ji, J.-P. Hong, S.-W. Jung, and S.-J. Ko, "Rethinking Coarse-to-Fine Approach in Single Image Deblurring." arXiv, Sep. 16, 2021.
[30] L. Chen, X. Lu, J. Zhang, X. Chu, and C. Chen, "HINet: Half Instance Normalization Network for Image Restoration." arXiv, May 01, 2022.
[31] D. Park, D. U. Kang, J. Kim, and S. Y. Chun, "Multi-Temporal Recurrent Neural Networks For Progressive Non-Uniform Single Image Deblurring With Incremental Temporal Training." arXiv, Nov. 17, 2019.
[32] K. Zhang et al., "Deblurring by Realistic Blurring," in 2020 IEEE/CVF Conference on Computer Vision and Pattern Recognition (CVPR), Seattle, WA, USA, Jun. 2020, pp. 2734–2743. doi: 10.1109/CVPR42600.2020.00281.
[33] X. Mao, Y. Liu, W. Shen, Q. Li, and Y. Wang, "Deep Residual Fourier Transformation for Single Image Deblurring." arXiv, Nov. 23, 2021.
[34] Ian Goodfellow, Yoshua Bengio, and Aaron Courville. 2016. Deep Learning. The MIT Press.
[35] O. Ronneberger, P. Fischer, and T. Brox, "U-Net: Convolutional Networks for Biomedical Image Segmentation." arXiv, May 18, 2015.
[36] A. G. Howard et al., "MobileNets: Efficient Convolutional Neural Networks for Mobile Vision Applications." arXiv, Apr. 16, 2017.
[37] M. Tan and Q. V. Le, "EfficientNet: Rethinking Model Scaling for Convolutional Neural Networks." arXiv, Sep. 11, 2020.
[38] M. Tan et al., "MnasNet: Platform-Aware Neural Architecture Search for Mobile." arXiv, May 28, 2019.
[39] Nah, S. , T. H. Kim , and K. M. Lee . "Deep Multi-scale Convolutional Neural Network for Dynamic Scene Deblurring." IEEE Computer Society, 10.1109/CVPR.2017.35. 2016.